

GW+EDMFT investigation of $\text{Pr}_{1-x}\text{Sr}_x\text{NiO}_2$ under pressureViktor Christiansson , Francesco Petocchi , and Philipp Werner 
Department of Physics, University of Fribourg, 1700 Fribourg, Switzerland (Received 9 September 2022; revised 16 December 2022; accepted 17 January 2023; published 30 January 2023)

Motivated by the recent experimental observation of a large pressure effect on T_c in $\text{Pr}_{1-x}\text{Sr}_x\text{NiO}_2$, we study the electronic properties of this compound as a function of pressure for $x = 0$ and 0.2 doping using self-consistent GW+EDMFT. Our numerical results demonstrate a nontrivial interplay between chemical doping and physical pressure, and small but systematic changes in the orbital occupations, local level energies, and interaction parameters with increasing pressure. The proper treatment of correlation effects, beyond density functional theory, is shown to play an important role in revealing these trends. While the pressure-dependent changes in the electronic structure of the undoped compound suggest a more single-band-like behavior in the high-pressure regime, a qualitatively different behavior is found in the doped system. We also point out that the fluctuations in the orbital occupations and spin states are not consistent with a single-band picture, and that at least a two-band model is necessary to reproduce the full result. This multiorbital nature manifests itself most clearly in the doped compound.

DOI: [10.1103/PhysRevB.107.045144](https://doi.org/10.1103/PhysRevB.107.045144)**I. INTRODUCTION**

Since the recent discovery of superconductivity in the infinite-layered phase of Sr-doped NdNiO_2 [1], an intense research effort, both on the experimental and theoretical side, has been devoted to understanding the electronic properties of this class of materials. In particular, the similarities and differences to the cuprate superconductors have received significant attention. In the mean time, the family of infinite-layered nickelates exhibiting superconductivity has grown to include Sr-doped PrNiO_2 [2,3], and both Sr- [4] and Ca-doped [5] LaNiO_2 . Furthermore, superconductivity has recently been discovered in finite-layered nickelates ($n = 5$ layers), in the absence of chemical doping [6], which provides an interesting additional avenue for exploring the pairing mechanism in this class of materials.

A widely debated but still not fully settled question concerns the single- versus multiorbital nature of these systems. Some groups [7–11] argue that the Ni $3d_{x^2-y^2}$ orbital is the main player and relevant for the observed superconductivity (as in the cuprates), while other groups [12–17] claim that the inclusion of additional Ni orbitals is necessary to accurately describe the low-energy physics. Other open questions range from the relevance of the in-plane oxygen orbitals in a multiorbital modeling [9], to the importance of the self-doping caused by the rare-earth atom layer separating the NiO_2 planes [18,19]. A recent review of the present understanding can be found, e.g., in Ref. [20].

Recently, Wang *et al.* [21] reported that upon applying pressure to doped $\text{Pr}_{1-x}\text{Sr}_x\text{NiO}_2$ ($x = 0.18$), the superconducting critical temperature T_c is enhanced from 18 K at ambient conditions to 31 K at 12.1 GPa, with no sign of saturation. This opens up an interesting prospect for experimentally reaching even higher values of T_c , similar to the

cuprates where the highest T_c values are also reached under pressure [22,23]. On the theoretical side the systematic trend with pressure provides a potentially fruitful venue to gain insights into the single- versus multiorbital question, and ultimately a deeper understanding of the underlying mechanism of superconductivity in the nickelates.

Some authors have considered an equivalent chemical pressure effect by altering the chemical composition leading to a change also in the c -lattice constant. In particular, a change in the rare-earth [24,25] in RNiO_2 was shown to result in large changes (Ref. [25] finds that the change from La to Y corresponds to a pressure of ~ 19 GPa), while additionally intercalating the structure with topotactic H in RNiO_2H results in small effects on the c -lattice parameter compared to the stoichiometric compound [26,27]. However, to our knowledge, only Been *et al.* [24], in their LDA + U [28] study of the effects of altering the rare-earth in infinite-layer nickelates, also performed a tentative comparison to a pressure-induced volume change without changing the chemical composition. The authors found that applying pressure results in a small increase of the hopping t (estimated from the $d_{x^2-y^2}$ bandwidth), although they concluded that a substantially larger effect is found by the substitution of the rare-earth.

Using an effective single-orbital description of the nickelates, Kitatani *et al.* [8] calculated T_c of Sr-doped NdNiO_2 by means of the dynamical vertex approximation [29] (D Γ A), predicting a superconducting dome which is in remarkably good agreement with that later found in experiments [30,31]. They furthermore argued that a decrease of the interaction-to-bandwidth ratio in their calculations would lead to an increase in T_c . It is therefore of interest to study the effect of pressure on the hopping t and effective interaction U to ascertain if such an effect would be consistent with the application of physical pressure in the nickelates.

In this work we use the recently developed multisite extension [15] of the multitier $GW+EDMFT$ method [32–35] to investigate the effects of pressure on the electronic properties of the infinite-layer nickelates. To emulate the effects of applying pressure, we assume the in-plane lattice constant to be fixed, and decrease only the out-of-plane lattice constant c (as speculated in Ref. [21]). We perform self-consistent $GW+EDMFT$ simulations both for a close-to-optimally doped ($x = 0.2$) and undoped ($x = 0$) $\text{Pr}_{1-x}\text{Sr}_x\text{NiO}_2$ system. To accurately capture possible multiorbital effects we use a low-energy model, obtained from downfolding an initial DFT [36,37] calculation, containing the full Ni $3d$ manifold and the Pr $5d_{xy}$ and $5d_{z^2}$ orbitals. We systematically study the effect of increasing physical pressure for both dopings and find qualitative differences between the two pressure responses. We show that a multiband picture is important for describing the local state fluctuations in both the undoped and doped systems. Intriguingly, however, the interplay between doping and pressure leads to an increasingly more single-band-like picture for the undoped system at high pressure, while this is not the case at (close-to) optimal doping. Here we instead find the multiorbital nature to be important to describe the evolution of the electronic properties over the considered pressure range.

The paper is organized as follows. In Sec. II we describe the DFT calculations used as the starting point for the many-body calculations, followed by an outline of the multisite extension to the multitier $GW+EDMFT$ method used in this work. In Sec. III we consider the effect of pressure on the electronic structure of the undoped and (close-to) optimally doped systems, and discuss what it implies for the single-versus multiorbital nature of the materials. In Sec. IV we summarize our findings and conclusions.

II. METHOD

A. DFT and technical details

In our approach we start from a DFT [36,37] calculation of $\text{Pr}_{1-x}\text{Sr}_x\text{NiO}_2$ in the infinite layered phase (space group $P4/mmm$). The crystal structure is depicted in Fig. 1(a), with Wyckoff position (0.0, 0.0, 0.0) (1a) for Ni, (0.5, 0.5, 0.5) (1d) for Pr, and (0.5, 0.0, 0.0) (2f) for O. We use the generalized gradient approximation (GGA) [38] as implemented in the full-potential linearized augmented plane-wave (FLAPW) code FLEUR [39] on a $16 \times 16 \times 16$ \mathbf{k} -point grid. The Sr-doping is simulated using the Virtual Crystal Approximation [40] (VCA), and due to a technical limitation in the FLAPW method a fraction of the Pr is replaced by the consecutive element in the series, keeping the valence electrons consistent with a Sr doping. Within this approach, which is needed to make the $GW+EDMFT$ calculations computationally feasible, we hence perform all of the calculations with the primitive unit cell and replace Pr with a virtual atom. A more proper inclusion of the full disorder in the system would be an interesting future project. To discern possible differences in the pressure effects related to the doping, we will consider the pressure evolution of both the close-to-optimally doped ($x = 0.2$) and the undoped ($x = 0$) compound.

The effect of increasing pressure is simulated by assuming the in-plane lattice constant $a = b = 3.91$ Å to be kept fixed,

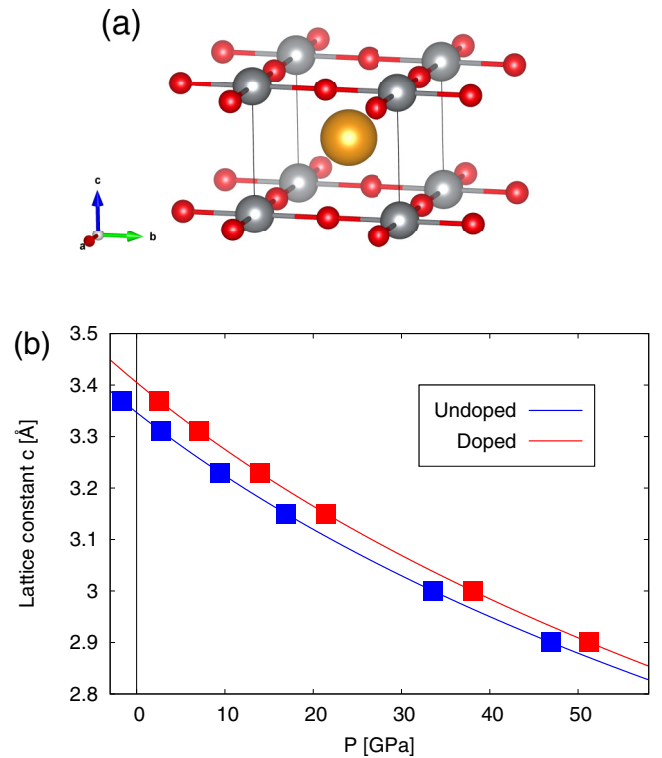


FIG. 1. (a) Crystal structure, drawn using VESTA [43], of PrNiO_2 in the infinite layered phase, with two Ni-O planes (gray and red, respectively) separated by the Pr (orange) layer shown. (b) Lattice constant c in Å as a function of pressure for undoped and doped ($x = 0.2$) $\text{Pr}_{1-x}\text{Sr}_x\text{NiO}_2$. The squares indicate the lattice constants used for the calculations in this work. Note that the calculated pressures are meant only to give a qualitative estimate of the pressure range, particularly for the doped compound.

similar to the approach in Ref. [24,41], and reducing only the out-of-plane lattice constant c . We give in Fig. 1(b) an estimate of the theoretical increase in pressure corresponding to the decrease in lattice constant obtained by fitting the DFT results with the Vinet equation of state [42]. The small offset of ~ 5 GPa between the two doping curves reflects the difference in the experimental lattice constants at zero pressure, which are reported to be $c = 3.31$ Å for the undoped compound and $c = 3.37$ Å at $x = 0.2$ doping [3]. We should note that due to our treatment of the doping using VCA, the pressure curve will not necessarily be quantitatively correct and Fig. 1(b) is only meant to give an estimate of the studied pressure range.

The smallest lattice constant considered, $c = 2.90$ Å, corresponds to a 12% (14%) reduction for the undoped (doped) compound, respectively, and is consistent with the $\sim 10\%$ decrease found in RNiO_2 across the Lanthanides series [24], confirming that our calculations in this pressure range are physically reasonable. However, the largest lattice constant considered in this work, $c = 3.37$ Å, is larger than the experimental value for the undoped compound at zero pressure. Accordingly it is estimated to correspond to a “negative” theoretical pressure.

To treat the Pr $4f$ electrons we use, similarly to our previous work [15], a manual core setup, and place the $4f^3$ electrons in the core. The remaining $4f$ states are treated with

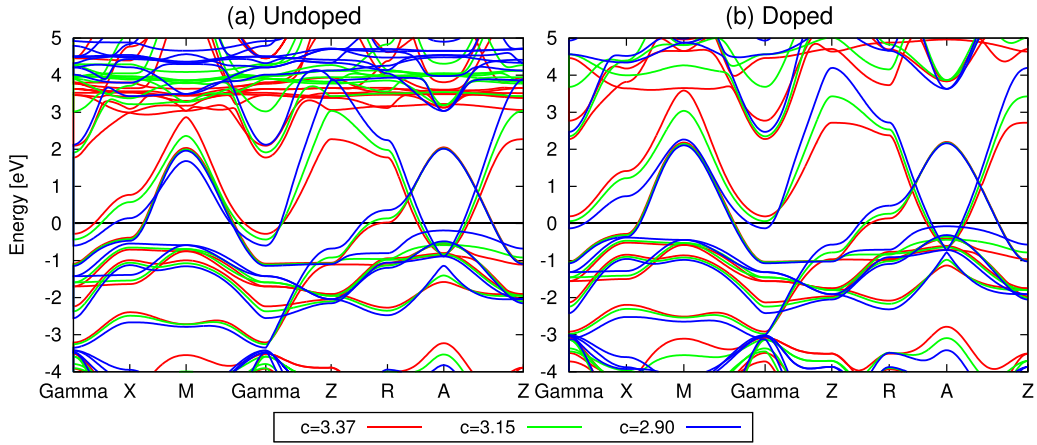


FIG. 2. The DFT band structure for the three indicated lattice constants c [for the equivalent pressure see Fig. 1(b)] in (a) the undoped and (b) the doped compound.

a self-consistent LDA + U + cRPA (constrained random-phase approximation [44]) scheme, where a cRPA calculation is performed iteratively to obtain a new interaction for the f -electrons in a LDA + U calculation until convergence. Due to the observation of superconductivity in nickelates with different rare-earths, it has been argued that these states are not very relevant for the pairing mechanism [20]. We therefore believe that this treatment should not affect our predictions.

The DFT band structures for both the undoped and doped compounds are shown in Fig. 2 as a function of decreasing lattice constant (increasing pressure). Interestingly, the self-doping Pr Fermi pocket around the Γ -momentum, which empties with increased Sr-doping x and disappears near optimal doping, is again partially reappearing upon increasing pressure in the doped compound, as more clearly shown in Fig. 3. The Pr pocket around the A -point instead slightly shrinks with increasing pressure. These DFT results are a first indication that chemical doping and physical pressure produce opposing effects. This phenomenon will become even more apparent in the discussions on the fully interacting system.

B. GW +EDMFT

In this section, we briefly outline the parameter-free multi-tier GW+EDMFT method and its recent multisite extension which has proven successful in the description of strongly correlated systems [15,34,35,45–47]. For a more detailed discussion on the method, we refer to Refs. [15,35].

Starting from the Kohn-Sham eigenvalues and eigenfunctions obtained from the DFT calculation described in the previous section, we define a low-energy model using maximally-localized Wannier functions (MLWFs) [48,49]. We adopt a seven-orbital model consisting of the five Ni d orbitals, and of Pr $5d_{xy}$ and $5d_{z^2}$. We then downfold the full DFT band structure to this low-energy subspace using a cRPA calculation [44] to obtain the effective bare interaction, $U_{\mathbf{q}}^{\text{cRPA}}(\omega)$, and a one-shot GW [50] calculation (G^0W^0) to obtain the noninteracting propagator in the low-energy space, $G_{\mathbf{k}}^0$. The cRPA and G^0W^0 calculations were performed using the SPEX [51] code with a $8 \times 8 \times 8$ \mathbf{k} -point grid and bands up to ~ 100 eV were used in the calculation of both the polarization and self-energy.

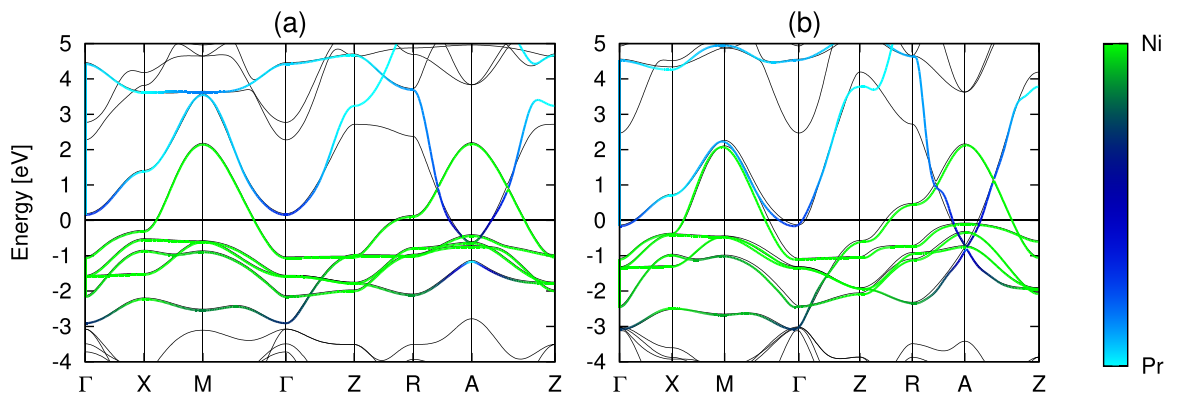


FIG. 3. DFT and Wannier band structure with the relative contribution from the Ni and Pr orbitals to the bands indicated for the doped system at (a) zero pressure ($c = 3.37 \text{ \AA}$) and (b) the maximum pressure considered in this work ($c = 2.90 \text{ \AA}$).

Within the multitier $GW+EDMFT$ formalism [35], we solve the problem self-consistently using the extended dynamical mean field theory [52,53] (EDMFT) self-consistency conditions $G^{\text{loc}} = G^{\text{imp}}$ and $W^{\text{loc}} = W^{\text{imp}}$, i.e., the local parts of the Green's function and screened interaction equal the corresponding results obtained from the solution of the EDMFT impurity problem. The interacting lattice Green's function, with the contributions from the different tiers, takes the form

$$G_{\mathbf{k}}^{-1} = i\omega_n + \mu - \varepsilon_{\mathbf{k}}^{\text{DFT}} + V_{\mathbf{k}}^{\text{XC}} - (\Sigma_{\mathbf{k}}^{G^0W^0} - \Sigma_{\mathbf{k}}^{G^0W^0}|_C) - (\Sigma_{\mathbf{k}}^{\text{sc}GW}|_C - \Sigma_{\text{loc}}^{\text{sc}GW}|_C) - \Sigma_{\text{loc}}^{\text{EDMFT}}|_C, \quad (1)$$

where μ is the chemical potential, and the DFT exchange-correlation potential $V_{\mathbf{k}}^{\text{XC}}$, contained in the Kohn-Sham single-particle energies $\varepsilon_{\mathbf{k}}^{\text{DFT}}$, has been replaced by the G^0W^0 self-energy $\Sigma_{\mathbf{k}}^{G^0W^0}$. The label C denotes the correlated space encompassing all seven orbitals considered in the low-energy model. The double counting between the tiers is well-defined [35], and the G^0W^0 contribution coming from the states within the low-energy space, $\Sigma_{\mathbf{k}}^{G^0W^0}|_C$, is replaced by the self-consistently obtained GW self-energy $\Sigma_{\mathbf{k}}^{\text{sc}GW}|_C$. An increased level of accuracy in the treatment of strong correlations is then achieved by replacing its local projection, $\Sigma_{\text{loc}}^{\text{sc}GW}|_C$, by the EDMFT impurity self-energy, $\Sigma_{\text{loc}}^{\text{EDMFT}}|_C$.

The contributions to the screening of the interaction from the different tiers and the corresponding double counting terms are similarly obtained,

$$W_{\mathbf{k}}^{-1} = v_{\mathbf{k}}^{-1} - (\Pi_{\mathbf{k}}^{G^0G^0} - \Pi_{\mathbf{k}}^{G^0G^0}|_C) - (\Pi_{\mathbf{k}}^{GG}|_C - \Pi_{\text{loc}}^{GG}|_C) - \Pi_{\text{loc}}^{\text{EDMFT}}|_C, \quad (2)$$

with the bare interaction $v_{\mathbf{k}}$ screened by the polarization contributions from the RPA ($\Pi_{\mathbf{k}}^{G^0G^0}$), self-consistent GW ($\Pi_{\mathbf{k}}^{GG}$), and the impurity $\Pi_{\text{loc}}^{\text{EDMFT}}$.

To handle the Ni and Pr sites, the multisite extension of $GW+EDMFT$ [15] defines separate fermionic and bosonic Weiss fields according to

$$\mathcal{G}_i = (\Sigma_i^{\text{imp}} + (G_i^{\text{imp}})^{-1})^{-1}, \quad (3)$$

$$\mathcal{U}_i = W_i^{\text{imp}}(1 + \Pi_i^{\text{imp}}W_i^{\text{imp}})^{-1}, \quad (4)$$

with the indices $i \in \{\text{Ni}, \text{Pr}\}$. This results in two separate impurity problems, with diagonal local (onsite) hybridization functions in the Wannier basis, which are solved using a continuous-time Monte Carlo solver [54,55] capable of treating dynamically screened interactions [56]. Since the nonlocal part of the problem is treated within the GW approximation, the orbitals centered on different sites are connected on this level. This leads to a coupling of Σ_i^{imp} and Π_i^{imp} for the two impurities through the lattice self-consistency equations [Eqs. (1) and (2)], with the EDMFT self-consistency conditions

$$G_i^{\text{imp}} = G_i^{\text{loc}}, \quad W_i^{\text{imp}} = W_i^{\text{loc}} \quad (5)$$

now having to be fulfilled for each of the two sites $i \in \{\text{Ni}, \text{Pr}\}$.

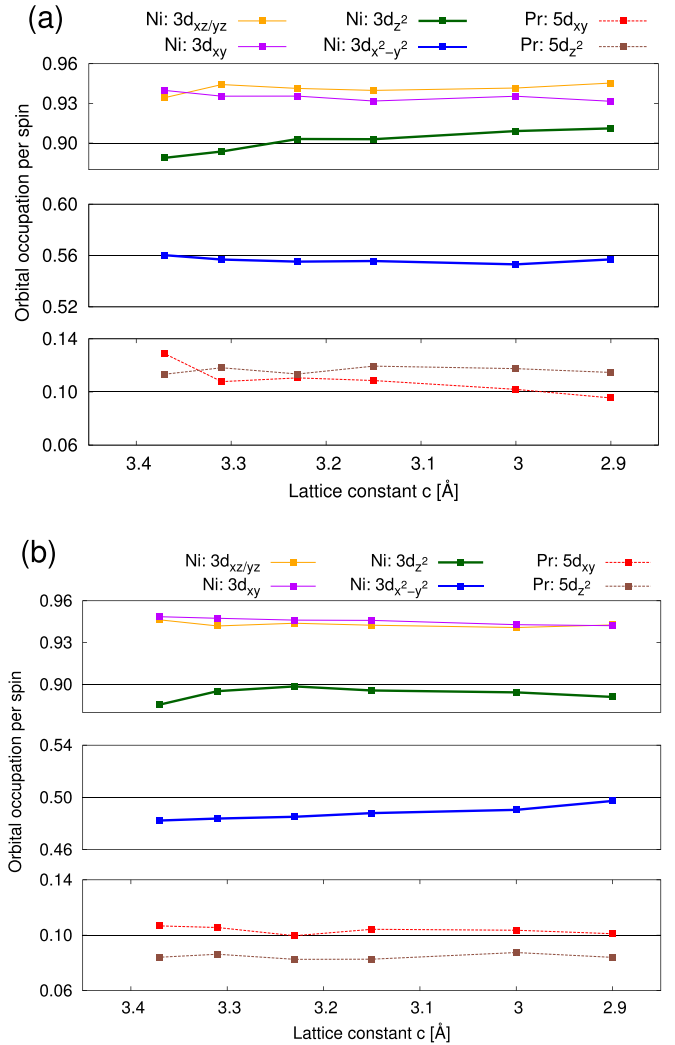


FIG. 4. Pressure dependence (in terms of the lattice constant c) of the orbital-resolved occupation per spin of the five Ni and the two Pr d -like orbitals included in the model for (a) the undoped and (b) the doped systems. The error bars given by the standard deviation for the averaged iterations is smaller than the dot sizes. Note the different ranges in the middle panels for the Ni $3d_{x^2-y^2}$ (blue) orbitals.

III. RESULTS

The $GW+EDMFT$ calculations were performed at temperature $T = 1/30$ eV on the $8 \times 8 \times 8$ \mathbf{k} -point grid from the downfolding, using the low-energy space defined in the previous section. The presented results have been obtained from an average over at least 10 consecutive converged iterations. We remind the reader that the $c = 3.37$ Å lattice constant is larger than the experimental value and hence corresponds to a theoretical negative pressure [Fig. 1(b)]. The corresponding data points are included for completeness, but left out of the discussions.

A. Orbital occupations

In Fig. 4 we show the pressure dependence of the orbital occupations in the undoped and doped compounds. From these orbital resolved occupations, we can deduce two main

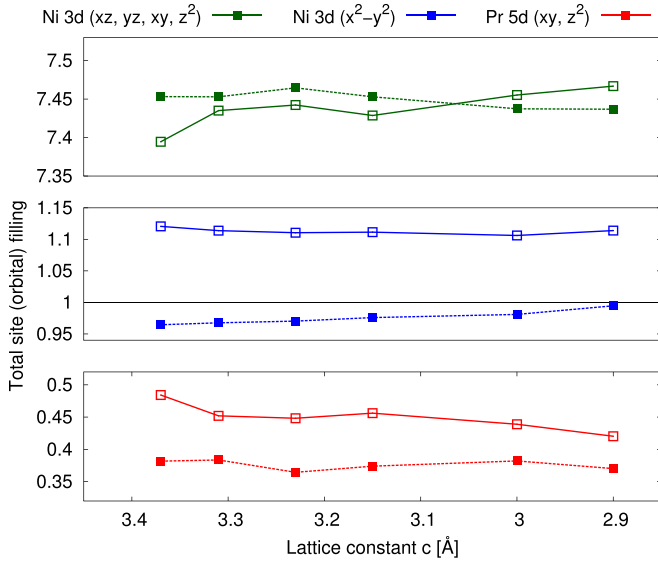


FIG. 5. Pressure dependence of the filling of the Ni and Pr sites (orbitals), in terms of the lattice constant c . We plot the total charge in the orbitals listed in the labels. The Ni $3d_{x^2-y^2}$ (close to half-filling) is shown separately from the other orbitals on the Ni site to clarify where the charge is moving. Full lines with empty squares show the results for the undoped compound and the dashed lines with filled squares show the results for the doped compound.

trends. In the undoped system, the Ni $3d_{x^2-y^2}$ filling remains pinned around a constant occupation of 0.56 electrons/spin, slightly higher than half-filling, and the main change is found in the Ni $3d_{z^2}$ -like orbital, whose filling monotonically increases with pressure. To better understand the charge redistribution, we look also at the site resolved occupations in Fig. 5, where the interesting Ni $3d_{x^2-y^2}$ orbital close to half-filling is shown separately. From this, it becomes clear that with increasing pressure, charge from the Pr site is transferred to the almost filled Ni orbitals, and that in particular the less occupied Ni $3d_{z^2}$ orbital is filled. The effect of increasing pressure is hence to suppress the self-doping, potentially making the system more single-band like.

The above trends in the undoped compound are in stark contrast to the behavior observed in the doped compound. Already the orbital resolved occupations indicate a transfer of charge away from the almost filled Ni orbitals to the Ni $3d_{x^2-y^2}$ orbital, shifting it closer to half-filling, while the occupation of the Pr site is only slightly decreasing with pressure, as is visible in Fig. 5. Furthermore, in the doped compound, the filling of the Ni $3d_{z^2}$ orbital displays a nontrivial pressure-dependence—at low pressures the occupation is increasing, while at higher pressures it empties out again, leading to the increase of the Ni $3d_{x^2-y^2}$ occupation toward half-filling at high pressure. This different behavior in the orbital occupations is a first indication of the importance of considering the presence of additional Ni orbitals to accurately capture the pressure dependence of the doped system, while this is less evident in the case of the undoped compound.

We note that unlike in our previous study of NdNiO₂ [15] (at the higher temperature $T = 1/10$ eV), we now find indications for a tendency to magnetic ordering at $T = 1/30$ eV.

TABLE I. Pressure dependence of the diagonal elements of the effective interaction $\mathcal{U}(i\omega_n = 0)$ in eV for the undoped system.

Orbital	3.37	3.31	3.23	3.15	3.00	2.90
Ni $3d_{xz/yz}$	5.53	5.49	5.47	5.53	5.48	5.47
Ni $3d_{xy}$	5.27	5.23	5.21	5.24	5.17	5.14
Ni $3d_{z^2}$	5.46	5.37	5.33	5.38	5.27	5.23
Ni $3d_{x^2-y^2}$	4.52	4.48	4.47	4.54	4.52	4.55
Pr $5d_{xy}$	1.95	1.99	1.98	1.92	1.93	1.90
Pr $5d_{z^2}$	1.84	1.88	1.95	1.87	1.94	1.91

This tendency toward magnetic ordering is larger in the doped compound, compared to the undoped system. However, since we performed the calculations for this study using the primitive cell, a more detailed analysis of the magnetic ordering is beyond the scope of this work, and we refer the reader to Ref. [20] and references therein.

B. Interaction parameters

A powerful feature of the GW+EDMFT formalism is that it provides a self-consistent calculation of the effective interaction parameters, which takes into account the screening by charge fluctuations in the low-energy subspace. In this section, we discuss the pressure-induced changes in these interaction parameters and how they are affected by doping. We focus mainly on the static effective bare onsite interaction, $\mathcal{U}(i\omega_n = 0)$, and briefly also discuss the Hund coupling, $\mathcal{J}(i\omega_n = 0)$. Information on the frequency-dependence can be found in Appendix A.

In the undoped case (Table I), the mostly occupied Ni orbitals (Ni $3d_{xz/yz}$, d_{xy} , d_{z^2}) show a small decrease of the interaction \mathcal{U} in the high-pressure regime, the most notable change being observed for the $3d_{z^2}$ orbital with a decrease of around 0.14 eV over the considered pressure range. The $d_{x^2-y^2}$ -like orbital (close to half-filling) instead exhibits a minor increase of ~ 0.07 eV in the interaction strength.

The situation is again very different for the doped system (Table II); the \mathcal{U} for the Ni $3d_{xz/yz}$ and d_{xy} orbitals remain approximately constant with only very small fluctuations with pressure, while the $3d_{z^2}$ orbital shows a decrease followed by an abrupt increase of around 0.14 eV at high pressures, where the orbital occupation is again decreasing (compare to Fig. 4). Such a nonmonotonic pressure effect on the effective interaction has previously been discussed in the context of cRPA [57], where the authors argued that the

TABLE II. Pressure dependence of the diagonal elements of the effective interaction $\mathcal{U}(i\omega_n = 0)$ in eV for the doped system.

Orbital	3.37	3.31	3.23	3.15	3.00	2.90
Ni $3d_{xz/yz}$	5.66	5.66	5.65	5.66	5.68	5.67
Ni $3d_{xy}$	5.18	5.19	5.20	5.20	5.20	5.16
Ni $3d_{z^2}$	5.79	5.75	5.70	5.68	5.82	5.79
Ni $3d_{x^2-y^2}$	4.43	4.46	4.49	4.51	4.59	4.63
Pr $5d_{xy}$	2.05	2.04	2.05	2.02	1.82	1.84
Pr $5d_{z^2}$	1.96	2.02	2.05	2.04	1.82	1.77

origin is a competing effect on the polarization from the band structure change and the orbital overlaps. These two effects tend to decrease and increase the polarization under pressure, respectively.

The $d_{x^2-y^2}$ orbital, however, displays a clear increase of 0.20 eV over the considered pressure range, almost three times the increase found in the undoped system, and again following the orbital occupation. This leads to the unexpected [8,58] result of an effective interaction \mathcal{U} which in the doped system is *larger* at high pressure than at ambient conditions.

On the almost empty Pr sites, in both the undoped and doped systems, the interaction on the $5d_{xy}$ orbitals is lowered with increasing pressure, by 0.09 and 0.20 eV respectively. While the undoped compound displays a monotonic behavior, the doped system exhibits an abrupt change in the high-pressure region. Similarly, the interaction for the $5d_{z^2}$ orbital in the undoped case fluctuates, while the doped system initially sees a slight increase with pressure followed by a rapid decrease of around 10%, without any discernible corresponding change in the orbital occupation (see Fig. 4).

We also note that U^{cRPA} for the important Ni $3d_{x^2-y^2}$ orbital follows approximately the same trend as discussed above for \mathcal{U} , but overestimates the interaction strengths (since it lacks the nonlocal screening from the low-energy subspace). For the undoped system at the experimental lattice parameters we have $U_u^{\text{cRPA}} = 4.97$ and for the doped system $U_d^{\text{cRPA}} = 5.00$ eV, compared to $\mathcal{U}_u = 4.48$ and $\mathcal{U}_d = 4.43$ eV. It is worth mentioning also the overestimation of U^{cRPA} for the Pr orbital, which is almost 40% larger than the self-consistently calculated local effective bare interaction \mathcal{U} (2.61 eV compared to 1.88 eV for the undoped, and 2.68 eV compared to 1.96 eV for the doped compound). These considerations emphasize again the importance of treating the low-energy physics beyond DFT and cRPA to accurately describe and compare the doped and undoped systems.

In Ref. [8] it was hypothesized that a smaller U/t ratio under pressure could be responsible for raising T_c based on DGA calculations for a single-orbital model. To elucidate this point, we compare the calculated in-plane hopping parameter for the Ni $3d_{x^2-y^2}$ electrons in the Wannier Hamiltonian, $t = -\mathcal{H}[\mathbf{R} = (1, 0, 0)]$, to the U^{cRPA} and \mathcal{U} interaction in Fig. 6.

The hopping t in the undoped system behaves qualitatively similar (although quantitatively different) to the Wannier estimate by Been *et al.* [24], who studied the dependence on the rare-earths and thereby effectively also changed the lattice parameter, with a nonmonotonic change (decrease followed by a subsequent increase) in the hopping over the pressure range. In the doped compound, we instead see a monotonic *decrease* in the hopping with pressure.

Although it is known that the effective interaction can increase with applied pressure [57], the observed behavior of the hopping parameter is rather counter-intuitive, as one would naively expect it to increase due to a larger overlap of the orbitals. We can however understand this trend by looking at the evolution of the Ni $3d_{x^2-y^2}$ Wannier functions. By estimating the degree of localization of the orbital from the spread functional in the MLWF formalism [48,59], we find that they become more localized with pressure, contrary to expectation. This results in smaller hopping integrals, and offers a simple explanation for the unexpected behavior. Together with the

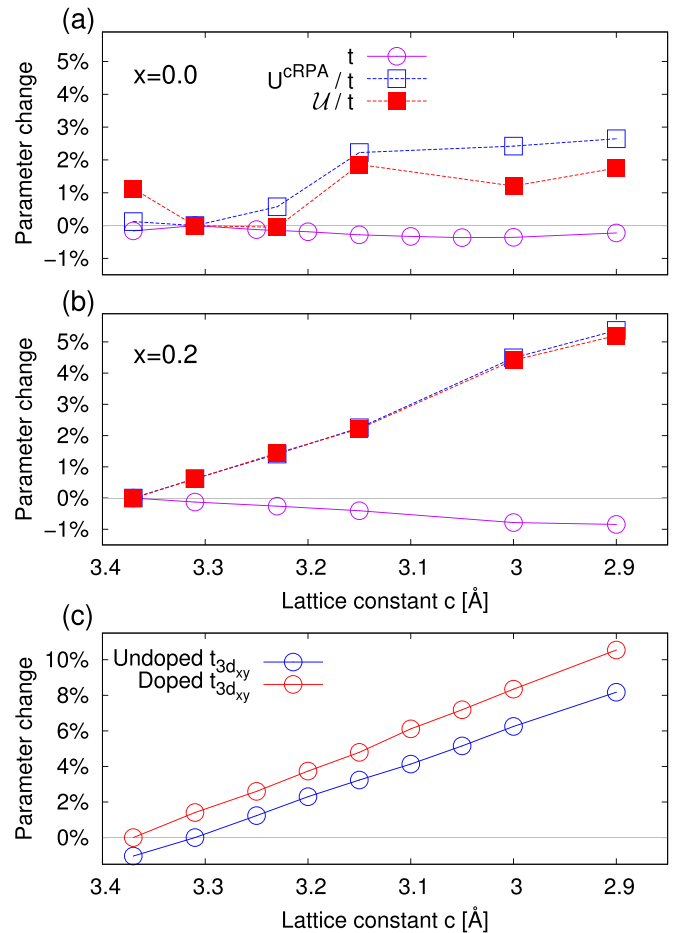


FIG. 6. Change in % from the zero-pressure values of the effective hopping t derived from the Wannier Hamiltonian, and the interaction-to-hopping ratios U^{cRPA}/t and U/t for Ni $3d_{x^2-y^2}$ as a function of pressure in (a) the undoped and (b) the doped compound. (c) Change compared to the zero-pressure result in the hopping t for Ni $3d_{xy}$ derived from the Wannier Hamiltonian.

previously discussed pressure dependence of the interaction, this leads to a significant difference in the doping behavior, with the undoped compound showing a more or less constant ratio of the interaction to hopping, U/t , while the doped compound exhibits a systematic *increase* with increasing pressure. All other Wannier functions instead exhibit the expected behavior of delocalization with increasing pressure, and as a consequence we observe for the other in-plane Ni $3d_{xy}$ orbital the expected increase in $t_{3d_{xy}}$; see Fig. 6(c).

Another estimate of the hopping parameters in undoped nickelates was given in Ref. [24] based on the band width of Ni $3d_{x^2-y^2}$ for NdNiO_2 , which they found to increase by $\sim 5\%$ over our studied pressure range. Using a similar estimate, we only find a change of 1–2%. This discrepancy can be traced back to the different treatment of the in-plane ($a = b$) lattice constant, which we have kept fixed. If we similarly also decrease the in-plane lattice constant by $\sim 1\%$, then we find an equivalent change of $\sim 4\%$ in the Ni $3d_{x^2-y^2}$ bandwidth. Using instead this estimated change in t for the undoped system would result in a slightly decreased ratio U/t at high pressure, while we would still not observe a decrease

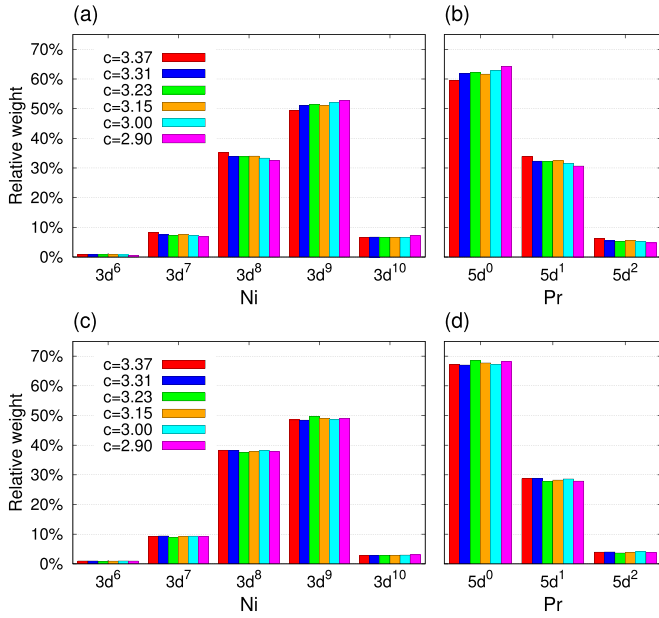


FIG. 7. EDMFT configuration statistics in the undoped system for (a) Ni and (b) Pr, and the doped system for (c) Ni and (d) Pr.

in the doped system – it would instead remain approximately constant (or slightly increase). With either way of estimating the hopping parameter, it becomes clear from the behavior of U/t that the undoped and doped systems react in qualitatively different ways to pressure. This makes it difficult to provide a simple explanation for the experimentally observed increase in T_c with increasing pressure based solely on this estimate.

Similar to NdNiO_2 [15], the calculated \mathcal{J} are slightly decreased under hole-doping. Contrary to the intraorbital interactions \mathcal{U} , however, there is no discernible pressure dependence. For completeness we list also some of the effective Hund couplings involving the Ni $3d_{x^2-y^2}$ -like orbital in Appendix C.

To wrap up the discussion on the interaction parameters we note that although the overall changes in the interaction and hopping parameters are small to moderate at most, we observe clear systematic trends. The results indicate a qualitatively different effect of pressure in the undoped and doped systems, in particular in the behavior of the interaction-to-hopping ratio, which must be taken into account when considering its implications for superconductivity.

C. Statistics

To further study the pressure evolution of PrNiO_2 and the single- versus multi-orbital characteristics of the system, we next discuss the statistics of the populated charge and spin sectors, which provides insights into the relevant atomic states. We show in Figs. 7 and 8 the occupation and spin statistics, respectively, for the undoped and doped compounds. These results can be obtained directly from the impurity models solved in the EDMFT calculations.

In agreement with our previous calculations for NdNiO_2 [15], the holes doped into the system empty the rare-earth site,

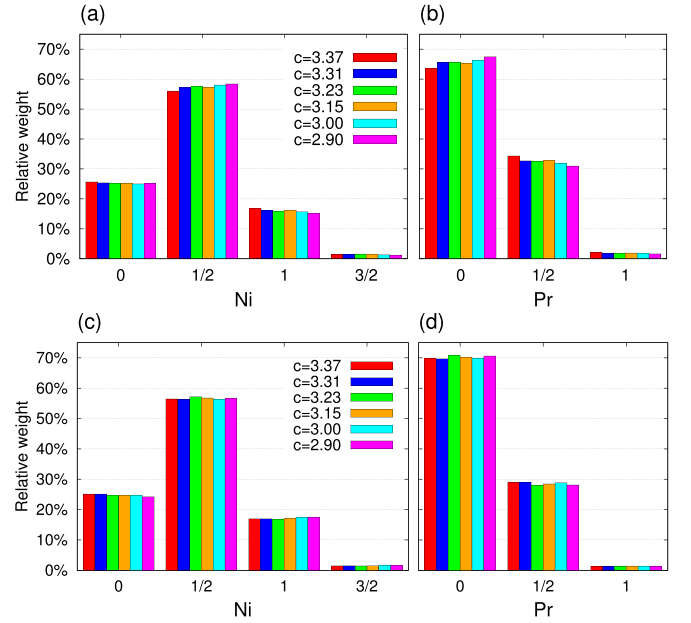


FIG. 8. EDMFT spin statistics for the spin-states $|S_z|$ in the undoped system for (a) Ni and (b) Pr, and the doped system for (c) Ni and (d) Pr.

as is evident from the increase in the Pr $5d^0$ configuration and corresponding decrease in the $5d^1$ configurations at fixed pressure (lattice constant). Upon increasing pressure, the undoped system shows weak indications for an increasingly single-band-like situation with an increase in the Ni $3d^9$ and Pr $5d^0$ configurations, while the fluctuations to Ni $3d^8$ and Pr $5d^1$ are suppressed accordingly—in agreement with the previous discussions of the orbital occupations. The effect of doping the system is an increase in the Ni $3d^7$ and $3d^8$ configurations, and a reduction in the $3d^9$ weights, in agreement with what would naively be expected. To interpret the pressure dependence and the trend toward a more or less single-band-like picture one needs to take into account the charge transfer between Pr and Ni. Here, we notice that in the doped compound, there is almost no pressure-dependent change in the Pr $5d^0$ weight. Hence, in the doped compound the self-doping from Pr is essentially unaffected by pressure, in contrast to the undoped compound where we observe a clear reduction. This is consistent with our previous observation that the orbital occupations are mostly redistributed locally (on the same site) by pressure in the doped system. Given this fact and the almost pressure-independent Ni $3d^n$ occupations, we conclude that the occupation statistics of the doped compound shows no hint of a more single-band-like behavior with increasing pressure.

The histograms of the spin states, shown in Fig. 8, indicate the importance of a multi-orbital description of both systems, because of the large weight from the high-spin configurations, as argued previously also for NdNiO_2 [15]. Similarly to the charge statistics, the undoped compound shows the behavior expected for an increasingly single-band-like description with increasing pressure, with a slight increase of the $|S_z^{\text{Ni}}| = \frac{1}{2}$ and $|S_z^{\text{Pr}}| = 0$ states, whereas the doped system again does not display any such systematic change.

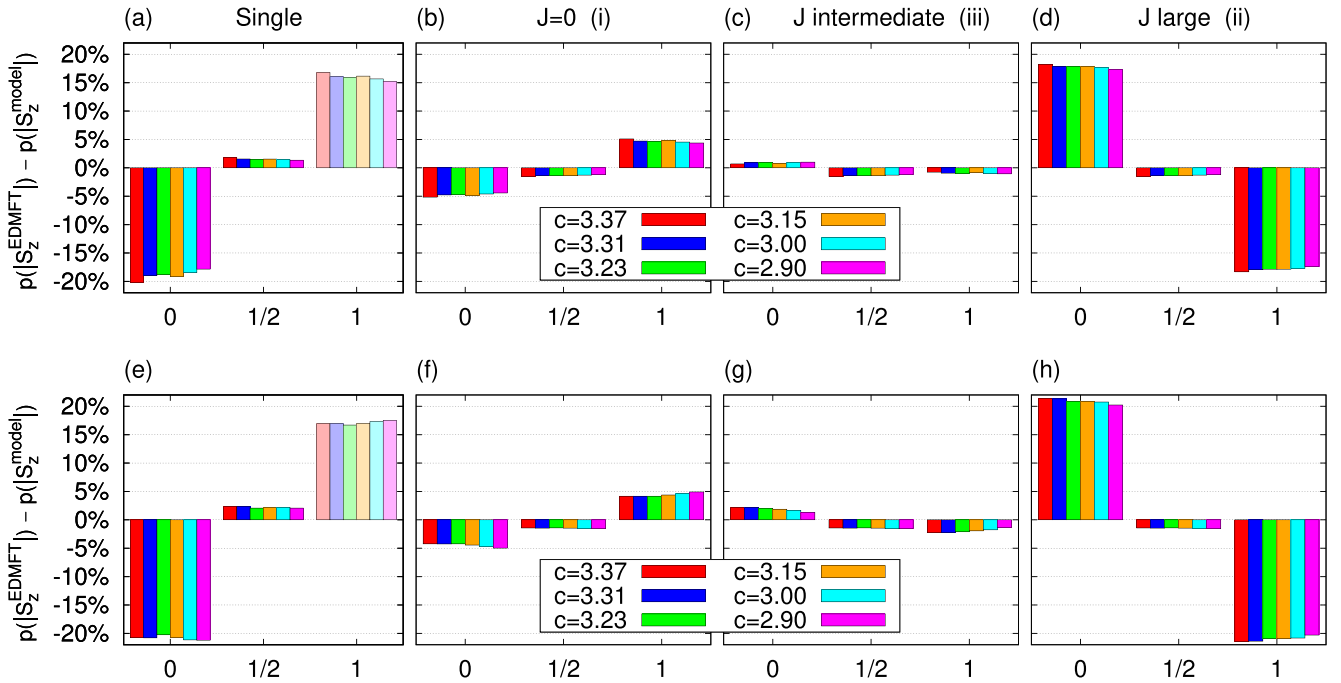


FIG. 9. Difference in the model estimates for the spin-state ($|S_z|=0, 1/2, 1$) weights from the full EDMFT results [$p(|S_z^{\text{EDMFT}}|) - p(|S_z^{\text{model}}|)$] for the undoped (a)–(d) and the doped (e)–(h) systems within the single- and two-orbital models described in the text. Since the probability for $|S_z| = 1$ in the one-orbital model is 0, the light shaded histograms in the left-most panels indicate the missing weight of the high-spin states.

To clarify the type of system represented by these histograms it is useful to compare them to the spin statistics estimated from a simple one- and two-orbital model, taking into account the constraints from the occupation statistics measured in the full interacting systems. We construct our two-orbital model by assuming that three of the Ni orbitals are fully occupied (the fluctuations to $3d^5$ and lower, not shown, are negligible). With this assumption the 0–4 electron sectors correspond to the Ni $3d^6$ – $3d^{10}$ states in the full calculation, respectively. We consider the following three cases: (i) negligible Hund coupling ($J = 0$) where the six possible 2-electron states contributing to $|S_z| = 0$ and $|S_z| = 1$ are equally probable, (ii) a large Hund coupling with only the high-spin configuration ($|S_z| = 1$) allowed in the two-electron sector, and (iii) an intermediate coupling, where we assume the probabilities of the low- and high-spin states to be equal, $p(|S_z| = 0) = p(|S_z| = 1)$. Model (iii) slightly favors the high-spin state over model (i). In the one-orbital model we additionally neglect the $3d^6$ and $3d^7$ states, and only represent the $3d^8$ – $3d^{10}$ configurations by the 0–2 electron sectors. Since the configurations included in the one-orbital model still account for more than 90% of the total weight measured in the full system, it should allow us to estimate if a single-orbital description is consistent with our results.

Figure 9 plots the difference between the benchmark EDMFT results and the model estimates for the relative weights. The contributions to the spin $|S_z| = 0, \frac{1}{2}, 1$ sectors of the various models are listed in Table III, and we use the calculated configuration probabilities shown in Fig. 7 for the corresponding probabilities $p(3d^n)$.

The first observation we can make is that the $|S_z| = \frac{1}{2}$ weight is accurately captured by all models, although slightly better in the two-orbital picture than in the single-orbital one. The high-spin $|S_z| = 1$ state, which is prominently populated in the EDMFT statistics, can obviously not be reproduced by the single-orbital model. However, more importantly, the single-orbital model significantly overestimates the $|S_z| = 0$ weight (by almost a factor of 2) for both dopings. The two-orbital model with $J = 0$ [model (i)], however, gives a relatively good agreement for both the $|S_z| = 0$ (overestimated) and $|S_z| = 1$ (underestimated) spin states. This is not the case for a large Hund coupling [model (ii)], which produces deviations on the same order as the single-orbital model, although in the opposite direction (underestimation of $|S_z| = 0$).

Taking into account competing effects which destabilize the high-spin state, e.g., crystal-field level-splittings, we can surmise that the real situation is most adequately described by model (iii), which in the half-filled case assigns equal probabilities to the high-spin and low-spin configurations. Indeed, as shown in Figs. 9(c) and 9(g), this model provides the best agreement with the EDMFT results, both for the undoped and doped systems. What these simple considerations show is that a single-orbital model cannot reproduce results which are consistent both with the occupation and spin statistics of the full model, while a two-orbital description is sufficient to reproduce both with good accuracy.

We would also like to briefly comment on the pressure dependence of the predictions from the different models. Starting with the the one-orbital model, for the undoped system we see a slight improvement with increasing pressure,

TABLE III. Contributions to the spin states $|S_z|$ from the n -electron sectors with probabilities $p(3d^n)$ for the models discussed in the text. The probabilities are taken from the EDMFT configuration statistics shown in Fig. 7.

	$n = 0$	$n = 1$	$n = 2$	$n = 3$	$n = 4$
One-orbital	$ S_z = 0 : p(3d^8)$	$ S_z = \frac{1}{2} : p(3d^9)$	$ S_z = 0 : p(3d^{10})$	—	—
Two-orbital (i) ($J = 0$)	$ S_z = 0 : p(3d^6)$	$ S_z = \frac{1}{2} : p(3d^7)$	$ S_z = 0 : \frac{4}{6}p(3d^8)$ $ S_z = 1 : \frac{2}{6}p(3d^8)$	$ S_z = \frac{1}{2} : p(3d^9)$	$ S_z = 0 : p(3d^{10})$
Two-orbital (ii) (J large)	$ S_z = 0 : p(3d^6)$	$ S_z = \frac{1}{2} : p(3d^7)$	$ S_z = 1 : p(3d^8)$	$ S_z = \frac{1}{2} : p(3d^9)$	$ S_z = 0 : p(3d^{10})$
Two-orbital (iii) (J intermediate)	$ S_z = 0 : p(3d^6)$	$ S_z = \frac{1}{2} : p(3d^7)$	$ S_z = 0 : \frac{3}{6}p(3d^8)$ $ S_z = 1 : \frac{3}{6}p(3d^8)$	$ S_z = \frac{1}{2} : p(3d^9)$	$ S_z = 0 : p(3d^{10})$

while the agreement for the doped system is equivalently worsened. This trend is shared by the prediction based on the two-orbital model without Hund coupling. The model with large coupling, although quantitatively not good, shows instead a comparable improvement for both the doped and undoped systems with increasing pressure. Model (iii), with intermediate Hund coupling effects, yields an improved description with increasing pressure for the doped system, while the undoped displays only very small changes without a clear trend.

Taken together, we interpret these results as further evidence for the multiorbital nature of PrNiO_2 ; while a trend toward a single-band picture is discernible in the undoped system with increasing pressure, this is not the case for the doped system. Irrespective of the doping, a single-band description cannot capture the effect of Hund coupling, which strongly affects the population of the different local states. Its effect remains significant even if one focuses only on the fluctuations within the $3d_{x^2-y^2}$ orbital.

D. Energy levels

We next discuss the renormalization of the local energy levels and the effect of pressure. In Fig. 10 we compare the DFT derived values, $\epsilon_{\text{DFT}} = \mathcal{H}_{\text{DFT}}(\mathbf{R} = 0) - \mu$, to the center of mass (CM) of the local spectral function $\epsilon_{\text{CM}} = \int \omega A(\omega) d\omega$, where $A(\omega)$ is the local spectral function corresponding to the full interacting Green's function in Eq. (1).

Already on the DFT level we see a clear pressure effect on the local Pr energy levels, which are lifted up with increasing pressure for both dopings. The Ni orbitals instead remain approximately constant in energy, the only notable difference being a slight reordering of the $3d_{xz/yz}$ and $3d_{xy}$ energy levels toward high pressure. This contrasts with the CM derived local energy levels, which reveal that the almost degenerate Ni $3d_{xz/yz}$, $3d_{xy}$, and $3d_{z^2}$ DFT levels get split by correlation effects, while pressure acts to move them closer together.

We can furthermore relate the pressure dependence of the filling on the Pr site, which we discussed earlier, to the CM energy levels. For the undoped compound, we find the difference in energy to the Ni $3d_{x^2-y^2}$ level to increase with pressure, following the previously noted trend of a decrease in the occupation. This results in a reduced self-doping. Conversely, for the doped compound the Pr are higher in energy, in agreement with the initially lower occupation. Furthermore, they do not display the same relatively large shifts with pressure as we

find without doping. Within DFT, however, these shifts appear to be comparatively large also in the doped system and could result in an overestimation of the pressure effects.

E. Pressure effect on O $2p$

Up until this point we have focused only on the Ni and Pr manifolds, while omitting the O p orbitals by integrating

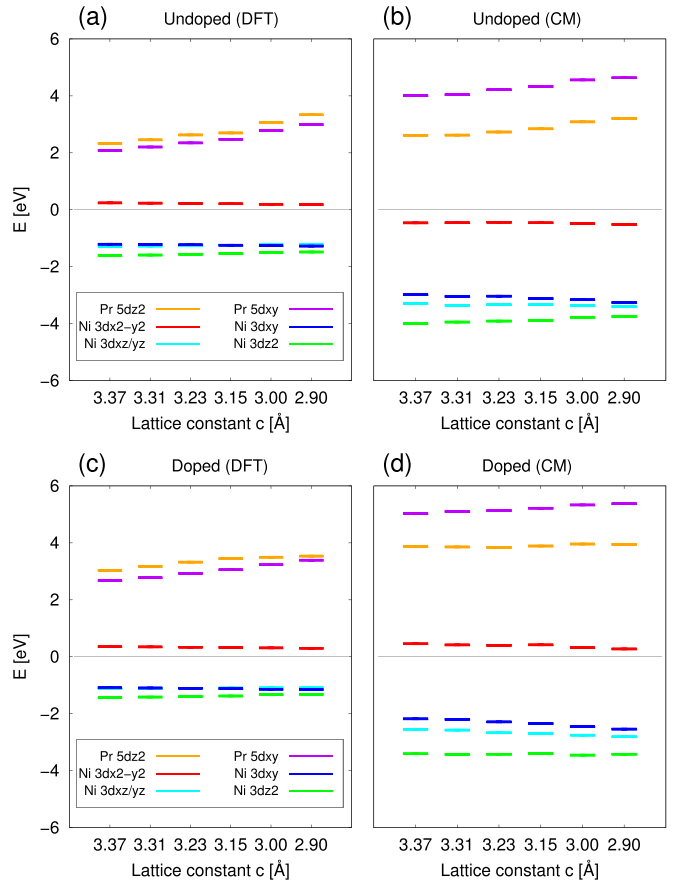


FIG. 10. Local energy level diagrams as a function of pressure (in terms of the lattice constant c) for the seven-orbital model. The different panels display results for the undoped compound derived from (a) DFT and (b) the center-of-mass of the spectral function in the interacting system, and for the doped compound derived from (c) DFT and (d) the center-of-mass of the spectral function in the interacting system.

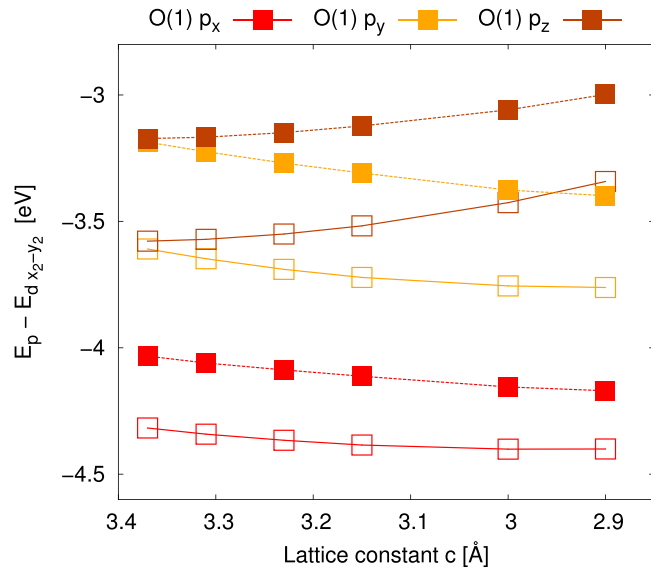


FIG. 11. O(1) p local energies relative to Ni $3d_{x^2-y^2}$ as a function of pressure (represented in terms of the lattice constant c). Full lines with empty squares show the results for the undoped compound and the dashed lines with filled squares those for the doped compound.

them out in the downfolding procedure following the DFT calculation. In this section we also briefly discuss the pressure effects on the O p local energy levels, derived by additionally including six oxygen-centered orbitals in the Wannierisation, yielding 13 orbitals in total. As expected, the larger energy window and number of bands reduces the spread for the Ni and Pr orbitals, and has the additional effect of lowering the local energies. We note, however, that the trends on the DFT level that we discussed previously remain unchanged, with the main difference being a slightly larger Ni $3d_{xz/yz}$ -Ni $3d_{xy}$ splitting.

In Fig. 11 we show the local energy levels ϵ_{DFT} , relative to Ni $3d_{x^2-y^2}$ (which remains approximately pinned close to the Fermi energy), for the $2p$ -like orbitals centered on the O(1) atom at (0.5, 0, 0). The equivalent Wannier functions for O(2) at (0, 0.5, 0) are related as: O(1) $p_x \leftrightarrow$ O(2) p_y and O(1) $p_y \leftrightarrow$ O(2) p_x , and the out-of-plane p_z for the two oxygens are equivalent.

Overall we note that the O $2p$ orbitals in the doped compound are higher in energy, compared to the undoped ones, on the order of ~ 0.5 eV. Additionally, we observe again two different systematic changes with increasing pressure; the in-plane orbitals (p_x and p_y) for both the doped and undoped systems are shifted down with pressure, while interestingly, the opposite trend is observed for the p_z orbitals which are shifted up in energy instead. As the in-plane orbitals are expected to hybridize more strongly with the Ni $3d_{x^2-y^2}$ orbital, this suggests a reduced involvement of the oxygen orbitals (with increasing pressure) in the mechanism underpinning the reported increase in T_c , at least on the DFT level. Taking into account also the O $2p$ orbitals in the low-energy space to self-consistently capture their effect would be needed to settle this question. Such an analysis is left for future work.

IV. SUMMARY AND CONCLUSIONS

To gain insights into the effects of physical pressure on the electronic structure of infinite layered nickelates, we used the parameter-free GW +EDMFT method to calculate orbital occupations, effective energy levels and effective interaction parameters. Our investigation focused on PrNiO₂, for which a substantial increase of T_c with increasing pressure has recently been reported in experiments [21]. The GW +EDMFT results also provided insights into the question of the single-versus multi-orbital nature of the system, and how this picture is affected by the application of pressure. The numerical calculations revealed quantitatively small changes, but clear systematic trends. One of the most interesting findings is the subtle interplay between chemical doping and pressure, which results in qualitatively different pressure evolutions for different doping levels, and subsequently different physical pictures.

We found several indications that the undoped system becomes more single-band-like at higher pressures. In the orbital occupations, one observes charge transfer mostly from Pr to the filled Ni orbitals, leaving the Ni $3d_{x^2-y^2}$ orbital essentially pinned at a fixed filling. Similarly the occupation and spin statistics in the high pressure region become increasingly more consistent with the behavior expected for a single-band system. The doped compound, however, does not display the changes that one would naively associate with an increasingly single-band-like picture. The charge transfer resulting from the application of pressure to a large extent occurs within the Ni $3d$ manifold. In particular we found a nonmonotonic change in the $3d_{z^2}$ occupation, which is responsible for moving the $3d_{x^2-y^2}$ orbital toward half-filling in the high-pressure regime. Such effects cannot be captured within a single-orbital picture. Our analysis further showed that a two-orbital model, with competition between Hund coupling and, e.g., crystal-field splitting effects, is the minimal model which satisfactorily reproduces the dominant fluctuations in the states of the full 7-orbital low-energy model. The reason is the significant weight of high-spin states, which affects the fluctuations even in the undoped system.

The effective local energy levels of the orbitals revealed an increase in the level splittings between Ni $3d_{x^2-y^2}$ and the Pr orbitals, consistent with a reduced self-doping from Pr under pressure in the undoped system, while the changes are less noteworthy in the doped compound. This is in agreement with our analysis of the orbital occupations. Our DFT analysis of the influence of pressure on the O $2p$ orbitals indicates that they are most likely not fundamental for understanding the pressure-induced increase in T_c , as the in-plane orbitals are systematically lowered in energy relative to the Ni $3d_{x^2-y^2}$ orbital which they would be expected to hybridize with. In the cuprate context, single-band behavior (in the sense of a weak hybridization between the $d_{x^2-y^2}$ and d_{z^2} orbitals) has been linked to high T_c values [60]. For this reason, it is tempting to interpret the increased T_c in Pr_{1-x}Sr_xNiO₂ under pressure as a consequence of the pressure-dependent level diagram (Fig. 10), which indicates an increasing decoupling of the $d_{x^2-y^2}$ orbital from the other orbitals, both at the DFT and GW +EDMFT level. While this trend looks consistent, the quantitative shifts in the doped interacting system are however

small and may not by themselves explain the large enhancement of T_c seen in the experiments.

The interaction parameters in the low-energy model exhibit small, but systematic changes over the considered pressure range. Particularly the calculated intraorbital interaction is of interest due to its possible relevance for the T_c estimate in a single-band picture based on $D\Gamma A$ [8]. While the cRPA estimate and the self-consistently computed \mathcal{U} show similar trends, the latter value is reduced as a result of low-energy screening processes, which again highlights the importance of an accurate treatment of the low-energy physics. Our calculations revealed that the expected decrease in the U/t ratio under pressure is not occurring, and we instead observe a substantial increase in the effective bare interaction with pressure. Depending on how we estimate the hopping parameter t , we can reach different conclusions depending on the doping. The estimate based on the Wannier Hamiltonian suggests a clear increase of U/t under pressure. In the undoped system, an estimate based on the bandwidth does instead lead to an approximately constant (or slightly decreasing) U/t , while intriguingly this is again not the case for the doped system, which still yields an increase in U/t (or an approximately constant U/t ratio if we also vary the in-plane lattice constants). These results suggest that an explanation of the experimentally observed T_c trend based on the *a priori* expected evolution of U/t can be misleading. However, further investigations of the screening and band widening effects are needed to settle the question.

To summarize, our results provide clear indications for a multiorbital nature of doped PrNiO_2 , which should manifest itself also under high pressure, while there are indicators for an opposite (more single-band-like) behavior in the undoped compound. Further experimental and theoretical investigations of the pressure effects at different doping levels, including the undoped compound, in PrNiO_2 and other nickelate superconductors would be helpful to establish systematic trends and to clarify the interplay between doping and physical pressure. Separate investigations of the pairing mechanism, which take into account the doping and pressure-dependent modifications of the screening and the level shifts revealed in this study, as well as the multiorbital nature of the material, are needed to clarify the effects of pressure on superconductivity.

ACKNOWLEDGMENTS

The calculations have been performed on the Beo05 cluster at the University of Fribourg. This work was supported by ERC Consolidator Grant No. 724103 and by the Swiss National Science Foundation via Grant No. 200021-196966.

APPENDIX A: FREQUENCY DEPENDENCE OF U

Because of dynamical screening processes, a properly defined local interaction for a low-energy effective theory has a substantial frequency-dependence. The significance of considering this effect can be clearly observed in Fig. 12 for a representative Ni- and Pr-like orbital, where there is more than a factor of 4 difference between the static ($\omega = 0$) and the bare (unscreened Coulomb interaction) limits.

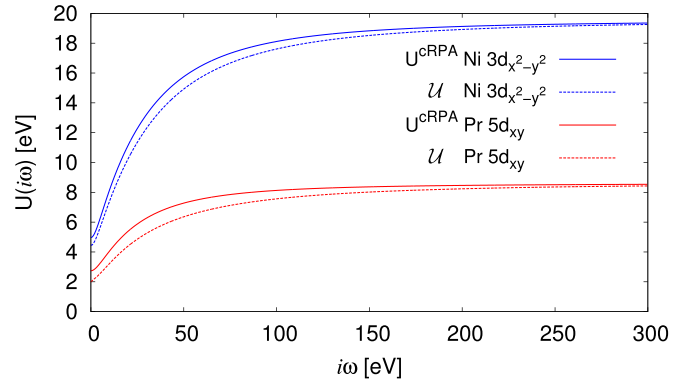


FIG. 12. Frequency dependence of the effective local bare interaction calculated within cRPA (full line) and the self-consistently calculated \mathcal{U} (dashed line) on the Matsubara axis for the Ni $3d_{x^2-y^2}$ (blue) and Pr $5d_{xy}$ (red) orbitals.

The renormalization of the effective static interaction, $\mathcal{U}(\omega = 0)$, due to nonlocal screening effects in the low-energy model, was discussed in the main text. We also observe here that these screening processes affect the frequency dependence of the effective interaction parameters beyond a simple shift of the static value. Such effects are fully captured within the self-consistent $GW+EDMFT$ formalism. As has been previously discussed in, e.g., Ref. [61], it is in principle possible to define an effective static interaction for the low-energy model which incorporates the frequency dependence, if at the same time one renormalizes the hopping parameters. In a multiorbital context, such a procedure however becomes complicated.

APPENDIX B: NONLOCAL INTERACTIONS FROM U^{cRPA}

Besides the treatment of the frequency dependence of the effective interaction, another strength of the $GW+EDMFT$ formalism is that it treats nonlocal components within GW .

To give an estimate of the importance of the nonlocal interactions in our calculations, we list in Table IV the spatial dependence of the static cRPA interaction for the $d_{x^2-y^2}$ -like orbital (in units of the lattice spacing). These results show that the nearest neighbor interaction is relatively weak (a factor of five smaller than the onsite interaction), although not completely negligible. The long-range effective bare interactions furthermore display a Coulomb-tail, as the low-energy metallic screening is removed within cRPA. The

TABLE IV. Spatial dependence of the static cRPA interaction in eV for the $d_{x^2-y^2}$ -like orbital in the plane. The vector \mathbf{R} is shown in units of the lattice spacing.

\mathbf{R}	(0,0,0)	(1,0,0)	(1,1,0)	(2,0,0)	(3,0,0)	(4,0,0)	(4,2,0)	(4,4,0)
U^{cRPA}	4.97	0.99	0.62	0.45	0.32	0.29	0.27	0.24

TABLE V. Pressure dependence of the effective Hund coupling $\mathcal{J}_{ab}(i\omega_n = 0)$ in eV between $a = \text{Ni } 3d_{x^2-y^2}$ and the other Ni orbitals $b = d_{z^2}, d_{xy},$ and $d_{xz/yz}$ for the undoped (u) and doped (d) systems in eV.

b	3.37	3.31	3.23	3.15	3.00	2.90
Ni $3d_{z^2}$ (u)	0.65	0.65	0.65	0.65	0.64	0.64
Ni $3d_{xy}$ (u)	0.36	0.36	0.36	0.37	0.37	0.36
Ni $3d_{xz/yz}$ (u)	0.60	0.60	0.60	0.61	0.61	0.61
Ni $3d_{z^2}$ (d)	0.65	0.65	0.65	0.65	0.65	0.65
Ni $3d_{xy}$ (d)	0.35	0.35	0.35	0.35	0.35	0.35
Ni $3d_{xz/yz}$ (d)	0.58	0.58	0.58	0.59	0.59	0.59

resulting nonlocal screening effects are quite significant, since they reduce the self-consistently computed bare onsite interaction \mathcal{U} compared to the cRPA estimate, as discussed in the main text.

APPENDIX C: PRESSURE DEPENDENCE OF \mathcal{J}

We list in Table V the pressure dependence of the effective Hund coupling $\mathcal{J}(i\omega_n = 0)$ between the Ni $3d_{x^2-y^2}$ and the other Ni orbitals. The couplings remain mostly unaffected by pressure, with maximum changes on the order of ~ 0.01 eV.

- [1] D. Li, K. Lee, B. Y. Wang, M. Osada, S. Crossley, H. R. Lee, Y. Cui, Y. Hikita, and H. Y. Hwang, *Nature (London)* **572**, 624 (2019).
- [2] M. Osada, B. Y. Wang, B. H. Goodge, K. Lee, H. Yoon, K. Sakuma, D. Li, M. Miura, L. F. Kourkoutis, and H. Y. Hwang, *Nano Lett.* **20**, 5735 (2020).
- [3] M. Osada, B. Y. Wang, K. Lee, D. Li, and H. Y. Hwang, *Phys. Rev. Mater.* **4**, 121801(R) (2020).
- [4] M. Osada, B. Y. Wang, B. H. Goodge, S. P. Harvey, K. Lee, D. Li, L. F. Kourkoutis, and H. Y. Hwang, *Adv. Mater.* **33**, 2104083 (2021).
- [5] S. Zeng, C. Li, L. E. Chow, Y. Cao, Z. Zhang, C. S. Tang, X. Yin, Z. S. Lim, J. Hu, P. Yang, and A. Ariando, *Sci. Adv.* **8**, eabl9927 (2022).
- [6] G. A. Pan, D. Ferenc Segedin, H. LaBollita, Q. Song, E. M. Nica, B. H. Goodge, A. T. Pierce, S. Doyle, S. Novakov, D. Córdova Carrizales, A. T. N'Diaye, P. Shafer, H. Paik, J. T. Heron, J. A. Mason, A. Yacoby, L. F. Kourkoutis, O. Erten, C. M. Brooks, A. S. Botana *et al.*, *Nat. Mater.* **21**, 160 (2022).
- [7] Y. Nomura, M. Hirayama, T. Tadano, Y. Yoshimoto, K. Nakamura, and R. Arita, *Phys. Rev. B* **100**, 205138 (2019).
- [8] M. Kitatani, L. Si, O. Janson, R. Arita, Z. Zhong, and K. Held, *npj Quant. Mater.* **5**, 59 (2020).
- [9] J. Karp, A. S. Botana, M. R. Norman, H. Park, M. Zingl, and A. Millis, *Phys. Rev. X* **10**, 021061 (2020).
- [10] J. Karp, A. Hampel, M. Zingl, A. S. Botana, H. Park, M. R. Norman, and A. J. Millis, *Phys. Rev. B* **102**, 245130 (2020).
- [11] K. Higashi, M. Winder, J. Kuneš, and A. Hariki, *Phys. Rev. X* **11**, 041009 (2021).
- [12] F. Lechermann, *Phys. Rev. B* **101**, 081110(R) (2020).
- [13] P. Werner and S. Hoshino, *Phys. Rev. B* **101**, 041104(R) (2020).
- [14] F. Lechermann, *Phys. Rev. X* **10**, 041002 (2020).
- [15] F. Petocchi, V. Christiansson, F. Nilsson, F. Aryasetiawan, and P. Werner, *Phys. Rev. X* **10**, 041047 (2020).
- [16] B. Kang, C. Melnick, P. Semon, S. Ryee, M. J. Han, G. Kotliar, and S. Choi, Infinite-layer nickelates as Ni-eg Hund's metals, [arXiv:2007.14610](https://arxiv.org/abs/2007.14610).
- [17] Y. Wang, C.-J. Kang, H. Miao, and G. Kotliar, *Phys. Rev. B* **102**, 161118(R) (2020).
- [18] K.-W. Lee and W. E. Pickett, *Phys. Rev. B* **70**, 165109 (2004).
- [19] Y. Gu, S. Zhu, X. Wang, J. Hu, and H. Chen, *Commun. Phys.* **3**, 84 (2020).
- [20] Y. Nomura and R. Arita, *Rep. Prog. Phys.* **85**, 052501 (2022).
- [21] N. N. Wang, M. W. Yang, Z. Yang, K. Y. Chen, H. Zhang, Q. H. Zhang, Z. H. Zhu, Y. Uwatoko, L. Gu, X. L. Dong, J. P. Sun, K. J. Jin, and J. G. Cheng, *Nat. Commun.* **13**, 4367 (2022).
- [22] L. Gao, Y. Y. Xue, F. Chen, Q. Xiong, R. L. Meng, D. Ramirez, C. W. Chu, J. H. Eggert, and H. K. Mao, *Phys. Rev. B* **50**, 4260 (1994).
- [23] M. Monteverde, C. Acha, M. Núñez-Regueiro, D. A. Pavlov, K. A. Lokshin, S. N. Putilin, and E. V. Antipov, *Europhys. Lett.* **72**, 458 (2005).
- [24] E. Been, W.-S. Lee, H. Y. Hwang, Y. Cui, J. Zaanen, T. Devereaux, B. Moritz, and C. Jia, *Phys. Rev. X* **11**, 011050 (2021).
- [25] F. Bernardini, A. Bosin, and A. Cano, *Phys. Rev. Mater.* **6**, 044807 (2022).
- [26] L. Si, W. Xiao, J. Kaufmann, J. M. Tomczak, Y. Lu, Z. Zhong, and K. Held, *Phys. Rev. Lett.* **124**, 166402 (2020).
- [27] O. I. Malyi, J. Varignon, and A. Zunger, *Phys. Rev. B* **105**, 014106 (2022).
- [28] V. I. Anisimov, F. Aryasetiawan, and A. I. Lichtenstein, *J. Phys.: Condens. Matter* **9**, 767 (1997).
- [29] G. Rohringer, H. Hafermann, A. Toschi, A. A. Katanin, A. E. Antipov, M. I. Katsnelson, A. I. Lichtenstein, A. N. Rubtsov, and K. Held, *Rev. Mod. Phys.* **90**, 025003 (2018).
- [30] D. Li, B. Y. Wang, K. Lee, S. P. Harvey, M. Osada, B. H. Goodge, L. F. Kourkoutis, and H. Y. Hwang, *Phys. Rev. Lett.* **125**, 027001 (2020).
- [31] S. Zeng, C. S. Tang, X. Yin, C. Li, M. Li, Z. Huang, J. Hu, W. Liu, G. J. Omar, H. Jani, Z. S. Lim, K. Han, D. Wan, P. Yang, S. J. Pennycook, A. T. S. Wee, and A. Ariando, *Phys. Rev. Lett.* **125**, 147003 (2020).
- [32] S. Biermann, F. Aryasetiawan, and A. Georges, *Phys. Rev. Lett.* **90**, 086402 (2003).
- [33] T. Ayrál, S. Biermann, and P. Werner, *Phys. Rev. B* **87**, 125149 (2013).
- [34] L. Boehnke, F. Nilsson, F. Aryasetiawan, and P. Werner, *Phys. Rev. B* **94**, 201106(R) (2016).
- [35] F. Nilsson, L. Boehnke, P. Werner, and F. Aryasetiawan, *Phys. Rev. Mater.* **1**, 043803 (2017).
- [36] P. Hohenberg and W. Kohn, *Phys. Rev.* **136**, B864 (1964).
- [37] W. Kohn and L. J. Sham, *Phys. Rev.* **140**, A1133 (1965).
- [38] J. P. Perdew, K. Burke, and M. Ernzerhof, *Phys. Rev. Lett.* **77**, 3865 (1996).
- [39] The FLEUR group, The FLEUR project, <http://www.flapw.de>.

- [40] L. Bellaïche and D. Vanderbilt, *Phys. Rev. B* **61**, 7877 (2000).
- [41] In this work, they also varied the in-plane lattice constant on the order of 1% to follow more closely the effect of the change in the rare-earth element.
- [42] P. Vinet, J. Ferrante, J. R. Smith, and J. H. Rose, *J. Phys. C* **19**, L467 (1986).
- [43] K. Momma and F. Izumi, *J. Appl. Crystallogr.* **44**, 1272 (2011).
- [44] F. Aryasetiawan, M. Imada, A. Georges, G. Kotliar, S. Biermann, and A. I. Lichtenstein, *Phys. Rev. B* **70**, 195104 (2004).
- [45] F. Petocchi, F. Nilsson, F. Aryasetiawan, and P. Werner, *Phys. Rev. Res.* **2**, 013191 (2020).
- [46] F. Petocchi, V. Christiansson, and P. Werner, *Phys. Rev. B* **104**, 195146 (2021).
- [47] V. Christiansson, F. Petocchi, and P. Werner, *Phys. Rev. B* **105**, 174513 (2022).
- [48] N. Marzari and D. Vanderbilt, *Phys. Rev. B* **56**, 12847 (1997).
- [49] A. A. Mostofi, J. R. Yates, Y.-S. Lee, I. Souza, D. Vanderbilt, and N. Marzari, *Comput. Phys. Commun.* **178**, 685 (2008).
- [50] L. Hedin, *Phys. Rev.* **139**, A796 (1965).
- [51] C. Friedrich, S. Blügel, and A. Schindlmayr, *Phys. Rev. B* **81**, 125102 (2010).
- [52] A. Georges, G. Kotliar, W. Krauth, and M. J. Rozenberg, *Rev. Mod. Phys.* **68**, 13 (1996).
- [53] P. Sun and G. Kotliar, *Phys. Rev. B* **66**, 085120 (2002).
- [54] P. Werner, A. Comanac, L. de' Medici, M. Troyer, and A. J. Millis, *Phys. Rev. Lett.* **97**, 076405 (2006).
- [55] H. Hafermann, P. Werner, and E. Gull, *Comput. Phys. Commun.* **184**, 1280 (2013).
- [56] P. Werner and A. J. Millis, *Phys. Rev. Lett.* **104**, 146401 (2010).
- [57] J. M. Tomczak, T. Miyake, R. Sakuma, and F. Aryasetiawan, *Phys. Rev. B* **79**, 235133 (2009).
- [58] K. Held, L. Si, P. Worm, O. Janson, R. Arita, Z. Zhong, J. M. Tomczak, and M. Kitatani, *Front. Phys.* **9**, 810394 (2022).
- [59] N. Marzari, A. A. Mostofi, J. R. Yates, I. Souza, and D. Vanderbilt, *Rev. Mod. Phys.* **84**, 1419 (2012).
- [60] H. Sakakibara, H. Usui, K. Kuroki, R. Arita, and H. Aoki, *Phys. Rev. Lett.* **105**, 057003 (2010).
- [61] M. Casula, P. Werner, L. Vaugier, F. Aryasetiawan, T. Miyake, A. J. Millis, and S. Biermann, *Phys. Rev. Lett.* **109**, 126408 (2012).